Bull Math Biol (2013) 75:2389–2409
DOI 10.1007/s11538-013-9897-3

Society for Mathematical Biology

ORIGINAL ARTICLE

A Phase-Field Model for Articular Cartilage Regeneration in Degradable Scaffolds

Ana Yun · Soon-Hyuck Lee · Junseok Kim

Received: 29 August 2012 / Accepted: 15 August 2013 / Published online: 26 September 2013

Abstract Degradable scaffolds represent a promising solution for tissue engineering of damaged or degenerated articular cartilage which due to its avascular nature, is characterized by a low self-repair capacity. To estimate the articular cartilage regeneration process employing degradable scaffolds, we propose a mathematical model as the extension of Olson and Haider's work (Int. J. Pure Appl. Math. 53:333–353, 2009). The simulated tissue engineering procedure consists in (i) the explant of a cylindrical sample, (ii) the removal of the inner core region, and (iii) the filling of the inner region with hydrogels, degradable scaffolds enriched with nutrients, such as oxygen and glucose. The phase-field model simulates the cartilage regeneration process at the scaffold-cartilage interface. It embeds reaction-diffusion equations, which are used to model the nutrient and regenerated extracellular matrix. The equations are solved using an unconditionally stable hybrid numerical scheme. Cartilage repair processes with full-thickness defects, which are controlled by properties of hydrogel materials and cartilage explant culture based on biological interest are observed. The implemented mathematical model shows the capability to simulate cartilage repairing processes, which can be virtually controlled evaluating hydrogel and cartilage material properties including nutrient supply and defected magnitude. In particular, the adopted methodology is able to explain the regeneration time of cartilage within hydrogel environments. With the numerical scheme, the numerical simulations are demonstrated for the potential improvement of hydrogel structures.

Keywords Phase-field model · Articular cartilage regeneration · Hydrogel · Reaction-diffusion model

A. Yun · J. Kim (✉)
Department of Mathematics, Korea University, Seoul 136-713, Republic of Korea
e-mail: cfdkim@korea.ac.kr

S.-H. Lee
Department of Orthopedic Surgery, Korea University College of Medicine, Seoul 136-705, Republic of Korea

1 Introduction

Articular cartilage is an avascular connective tissue, part of a complex bearing system characterizing diarthrodial joints, capable to provide load support for an enormous range of loading conditions. The impossibility to self-regenerate, due to the absence of blood vessels, drastically limits auto-repairing processes. Tissue engineering using scaffolds promote chondrocyte differentiation and the formation of cartilage matrix, inhibit chondrocyte proliferation, which result in the regeneration of defective cartilage (Grote et al. 2011; Temenoff and Mikos 2000). Hydrogels, biodegradable and biocompatible materials, are largely investigated for tissue engineering applications (Betre et al. 2002; Elisseeff et al. 1999; Nettles et al. 2004; Nguyen and West 2002; Noguchi et al. 1991; Stile et al. 1999). After implantation, hydrogels slowly degrade by cellular biosynthesis and proliferation, until the hydrogel is completely replaced by the cartilage (Davis et al. 2003; Ossendorf et al. 2007; Rydholm et al. 2005; Wilson et al. 2002) (see Fig. 1 from Jackson et al. 2001).

To explain experimental results such as Kuo and Tsai (2010)'s work, a mathematical modeling can be a useful tool as it is enable to predict spatial and temporal control of cartilage repair process (Trewenack et al. 2009) and efficient compared to expensive experimental studies (Sanz-Herrera et al. 2009). For this purpose, mathematical models for an in vitro experiment are studied for controlling the regeneration time and the potential improvement of hydrogel structures. As articular cartilage is avascular, it is natural to consider a full-thickness defect and we consider a cylindrical cartilage-hydrogel explant culture. The inner core of the cylindrical cartilage-hydrogel is removed and is filled with nutrient rich hydrogel. As the movement of molecules such as nutrients, wastes, oxygen, and matrix macromolecules through the tissue occurs by diffusion (Darling and Athanasiou 2003; Leddy and Guilak 2003; Burkitt et al. 1993), the molecular diffusion of nutrients stimulates the proliferation of chondrocytes, the cellular component of cartilage, and matrix synthesizes in reaction process (Galban and Locke 1997; Sengers et al. 2007; Wilson et al. 2007), a system of reaction-diffusion models (Glimm et al. 2012; Murray 2002) for nutrient and matrix accumulation is considered for the mathematical modeling.

In this paper, the phase-field model is proposed for articular–cartilage regeneration in hydrogels as an extension research of Olson and Haider's work (Olson and Haider 2009). They studied the reaction phenomena at the hydrogel–cartilage interface by idealizing the localized interface which is mathematically modeled by the level set method and is coupled with the reaction-diffusion system for the nutrient concentration and the newly generated matrix. The level set method, defined in Eulerian description of a free moving interface, represents an interface as the zero level set of a continuous function using the signed distance function, follows the movement of interface by the velocity and keeps interface integrity. The level set method converts the geometric problem into a partial differential equation to solve the geometric problem (Min 2010). However, the level set method has a restriction in numerical stability as it generally uses a numerical scheme such as an explicit scheme, suffers from the renormalization procedure (Gao et al. 2009).

We model the accumulation of newly generated ECM and the degradation of a scaffold in an cylindrical in vitro articular cartilage as the phase change by using

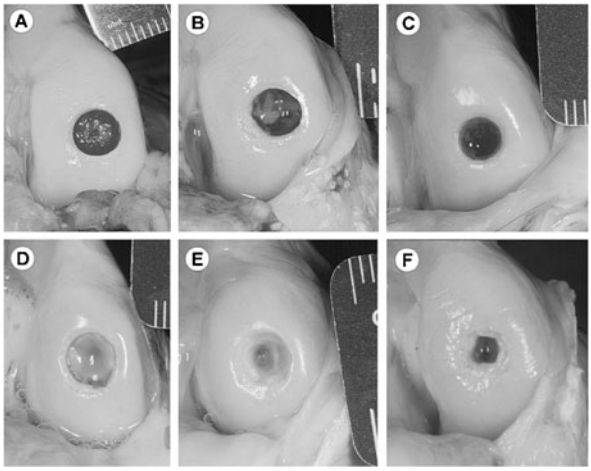

Fig. 1 Articular cartilage regeneration in the medial femoral condyle. **A**: Initial (immediately after creation of the lesion), **B**: 1 week, **C**: 2 weeks, **D**: 6 weeks, **E**: 24 weeks, and **F**: 52 weeks (Reprinted from Jackson et al. (2001), with pre-permission from the J. Bone Joint Surg. Am.)

a modified Allen–Cahn equation which is a type of phase-field method (Shirakawa and Kimura 2005) considering cartilage and hydrogel as separated phases. For the biological tissue, the phase-field model has the advantages of considering topological changes and allowing the employment of complex material properties (Yang et al. 2006). We propose an unconditionally stable hybrid method to solve the phase-field model. The proposed numerical scheme is efficient as the hybrid method uses an implicit scheme and analytical solutions.

Moreover, biological reaction terms are added and diffusions are treated as a function of the order parameter of the phase-field. For the reaction term, a well-mixed population model (Kooi et al. 1998) is implemented as we focus on the kinetics between nutrients and proliferation of matrix. We employ an unconditionally stable hybrid method to solve the reaction-diffusion system. Based on hydrogel materials and cartilage explant culture, parameters are varied to investigate spatial and temporal control of cartilage repair process. Considering the parameter set compared with the level set method and allowing the employment of complex material properties, we focus on the regeneration time of cartilage within hydrogel environments and the potential improvement of hydrogel structures.

2 The Mathematical Model

In this modeling approach, in vitro cartilage regeneration in a cylindrical tissue explant is assumed. The core of the cartilage damaged sample has been filled with a nutrient enriched hydrogel, such as photocrosslinkable hyaluronan (Nettles et al. 2004), polylactic acid (PLA), and elastin-like polypeptide (ELP). Nutrient diffusion into the cartilage stimulates cell proliferation and cellular biosynthesis of ECM. Then the newly synthesized ECM reacts to replace the hydrogel with newly formed ECM having chondrocytes. The complex biological problem is simplified as the mathematical model especially a reaction diffusion system with spatial and temporal evolutions for the nutrient concentration (N) and the newly generated ECM (M). The reaction

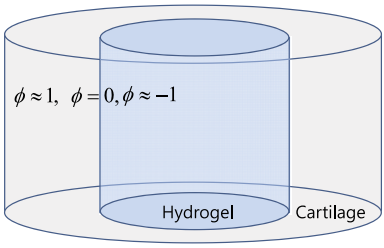

Fig. 2 Schematic illustration of the cartilage-hydrogel aggregate

phenomena at the hydrogel–cartilage interface are locally defined with the thin interface which is coupled with N and M.

We consider an order parameter ϕ, the difference between the concentrations of the two components in a mixture, which indicates cartilage-hydrogel as phases. The cartilage and hydrogel regions correspond to $\phi \approx 1$ and $\phi \approx -1$, respectively. The zero level set $\phi = 0$ is the location of the interface (Fig. 2).

Define N^* $(\mathrm{kg\,m^{-3}})$ and M^* $(\mathrm{kg\,m^{-3}})$ as homeostasis concentrations of N and M, respectively. We denote that the maximal capacity of M as $M_{\max}$. Then a reaction-diffusion system depending on a space and time for a nutrient concentration N $(\mathrm{kg\,m^{-3}})$ and a newly generated ECM (extracellular matrix) M $(\mathrm{kg\,m^{-3}})$ is considered as (Galban and Locke 1997; Olson and Haider 2009):

$$\frac{\partial N}{\partial t} = \nabla \cdot \big(D_N(\phi)\nabla N\big) - K_N(\phi)\big(N - N^*\big)(M_{\max} - M), \tag{1}$$

$$\frac{\partial M}{\partial t} = \nabla \cdot \big(D_M(\phi)\nabla M\big) + K_M(\phi)\big(N - N^*\big)(M_{\max} - M), \tag{2}$$

where D_N $(\mathrm{m^2\,s^{-1}})$ and D_M $(\mathrm{m^2\,s^{-1}})$ are diffusion coefficients of nutrients and ECM, respectively.

Note that nutrient transport and synthesis of ECM follows diffusion of molecules. Moreover, cellular consumption of nutrients and synthesis of ECM are modeled as the well-mixed population models (Kooi et al. 1998) for the reaction terms. This modeling approach is realistic as the nutrient consumption and matrix aggregation are simultaneously occurred (Freed et al. 1994). $D_N(\phi) = 0.5D_N^-(1-\phi) + 0.5D_N^+(1+\phi)$, $D_M(\phi) = 0.5D_M^-(1-\phi) + 0.5D_M^+(1+\phi)$. D_N^-, D_M^- are defined in the hydrogel region and D_N^+, D_M^+ are coefficients for the cartilage region. When nutrient supplies enough to reach the homeostasis N^*, diffusion dominates to N and M, and the ECM has its maximum to M^* by reaction terms in Eqs. (1) and (2).

Nutrients are consumed with the nutrient utilization rate $K_N(\phi)$ (s^{-1}) and the ECM concentration aggregates with the rate $K_M(\phi)$ (s^{-1}). The reaction term of N diminishes at a rate proportional to the matrix $M_{\max} - M$, nutrient, and the consumption rate $K_N(\phi)$ whereas the reaction term of M generates at a rate proportional to $N - N^*$, and the aggregation rate $K_M(\phi)$.

For the consumption rate $K_N(\phi)$ and the aggregation rate $K_M(\phi)$, which have different values between the cartilage and the hydrogel region by means of ϕ, we let

$$K_N(\phi) = k_N\frac{1+\phi}{2}, \qquad K_M(\phi) = k_M\frac{1+\phi}{2}, \tag{3}$$

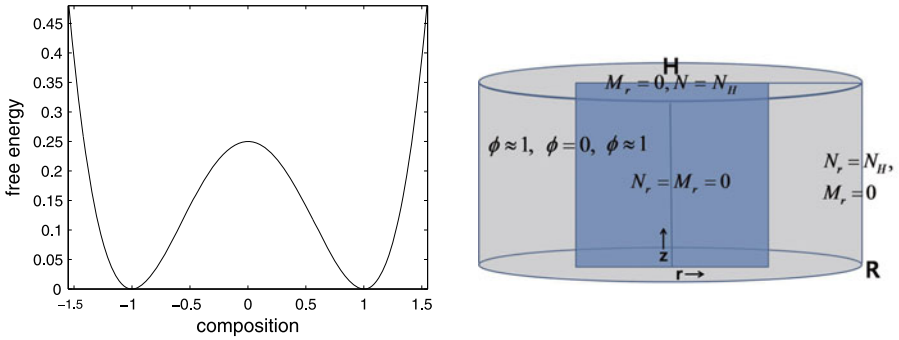

(a) (b)

Fig. 3 (**a**) Free energy, $F(\phi) = 0.25(\phi^2 - 1)^2$. (**b**) Axisymmetric domain with boundary conditions

respectively. In this expression, $K_N(\phi) = K_M(\phi) = 0$ are naturally assumed in the unseeded hydrogel region.

For the governing equation of the order parameter ϕ, we propose the modified Allen–Cahn equation considering M as a diffuse mobility factor. As the Allen–Cahn equation shows inherent motion by mean curvature, the additional directional anisotropy of the order parameter ϕ is incorporated through M (Taylor and Cahn 1998). It should be noted that the interfacial effect is added as a term $\beta M F(\phi)$. The proposed governing equation for ϕ is

$$\phi_t = -\alpha\big(M^* + M\big)\left(\frac{F'(\phi)}{\epsilon^2} - \Delta\phi\right) + \frac{\sqrt{2}\beta}{2\epsilon}\big(M^* + M\big)\sqrt{F(\phi)}, \tag{4}$$

where $F(\phi) = 0.25(\phi^2 - 1)^2$, positive constants α, β, and ϵ. Note that α and β are the rate controlling the degradation of the hydrogel. The Helmholtz free energy density $F(\phi)$ is shown in Fig. 3(a). ϵ is the gradient energy coefficient related to the thickness of the interfacial transition of the phase-field, α is the parameter corresponding to the Allen–Cahn equation which influences to the curvature, and β affects to the interfacial transposition. The initial conditions are given by

$$N(r, z, 0) = \begin{cases} N_H, & 0 < r < a, \\ N^*, & a < r < R, \end{cases} \tag{5}$$

$$M(r, z, 0) = 0, \tag{6}$$

where N_H is the initial nutrient concentration of the nutrient-rich hydrogel.

The boundary conditions of N are given as Dirichlet boundary, interpreted as nutrient source, at $z = H$ and $r = R$, which are upper and right-hand sides, respectively. Nutrient source affects to the spatial and temporal regeneration which will be discussed in Sect. 4.1. The boundary conditions for N, M, and ϕ are imposed as no flux which is zero Neumann boundary. Our axisymmetric domain with boundary conditions is depicted in Fig. 3(b).

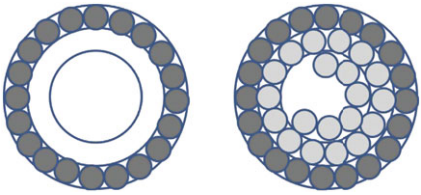

Fig. 4 Schematic of curvature-dependent cell aggregation. The first cell layer (*dark gray circles*, *left-hand side*) and the first and second cell layers (*right-hand side*, *the second layer* is represented with *bright gray circles*) with the same cell densities

To see the curvature effect in the axisymmetric domain, a schematic representation of curvature-dependent cell aggregation is depicted by circles in Fig. 4. The left-hand side of Fig. 4 shows the first cell layer (darker gray circles) and the right-hand side shows the first and second cell layers where the second cell layer is represented with brighter gray circles. Though two layers have the same cell densities, the second layer goes inward rapidly by the curvature effect. Inspection of Fig. 4 reveals that the aggregation speeds up to the core which will be observed in simulations in Sect. 4.

The nondimensional parameters are employed to have non-dimensional N, M, and D_N for the numerical calculations:

$$\widetilde{N} = \frac{N}{N^*}, \qquad \widetilde{M} = \frac{M}{M^*}, \qquad \widetilde{\Gamma}_N(\phi) = \frac{K_N(\phi)N^*}{D_N^-}, \qquad \widetilde{\Gamma}_M(\phi) = \frac{K_M(\phi)M^*}{D_N^-},$$
$$\widetilde{D}_N(\phi) = \frac{D_N(\phi)}{D_N^-}, \qquad \widetilde{D}_M(\phi) = \frac{D_M(\phi)}{D_N^-}, \qquad \widetilde{\gamma}_N = \frac{k_N}{D_N^-}, \tag{7}$$
$$\widetilde{\gamma}_M = \frac{k_M}{D_N^-}, \qquad \delta = \frac{M_{\max}}{M^*}, \qquad \widetilde{t} = tD_N^-.$$

Then we have the governing equations in the axisymmetric form:

$$\frac{D_N^- N^* \partial \widetilde{N}}{\partial t} = \frac{N^*}{r}\left(D_N^- \widetilde{D}_N(\phi) r \widetilde{N}_r\right)_r + N^*\left(D_N^- \widetilde{D}_N(\phi)\widetilde{N}_z\right)_z$$
$$- \frac{D_N^- \widetilde{\Gamma}_N(\phi)}{N^*}\left(N^*\widetilde{N} - N^*\right)\left(M^*\delta - M^*\widetilde{M}\right), \tag{8}$$
$$\frac{D_N^- M^* \partial \widetilde{M}}{\partial t} = \frac{M^*}{r}\left(D_N^- \widetilde{D}_M(\phi) r \widetilde{M}_r\right)_r + N^*\left(D_N^- \widetilde{D}_M(\phi)\widetilde{M}_z\right)_z$$
$$+ \frac{D_N^- \widetilde{\Gamma}_M(\phi)}{M^*}\left(N^*\widetilde{N} - N^*\right)\left(M^*\delta - M^*\widetilde{M}\right), \tag{9}$$
$$\frac{\partial \phi}{\partial t} = -\alpha\left(\delta M^* + \widetilde{M}M^*\right)\left(\frac{F'(\phi)}{\epsilon^2} - \Delta\phi\right)$$
$$+ \frac{\sqrt{2}\beta}{2\epsilon}\left(\delta M^* + \widetilde{M}M^*\right)\sqrt{F(\phi)}. \tag{10}$$

The governing equations are re-written omitting the tilde notation, the governing equations on the domain $\Omega = (0, 1) \times (0, H/R)$ are:

$$\frac{\partial N}{\partial t} = \frac{1}{r}\big(D_N(\phi) r N_r\big)_r + \big(D_N(\phi) N_z\big)_z - \Gamma_N(\phi)(N-1)(\delta - M), \tag{11}$$

$$\frac{\partial M}{\partial t} = \frac{1}{r}\big(D_M(\phi) r M_r\big)_r + \big(D_M(\phi) M_z\big)_z + \Gamma_M(\phi)(N-1)(\delta - M), \tag{12}$$

$$\frac{\partial \phi}{\partial t} = -\alpha(\delta + M)\left(\frac{F'(\phi)}{\epsilon^2} - \Delta\phi\right) + \frac{\sqrt{2}\beta}{2\epsilon}(\delta + M)\sqrt{F(\phi)}. \tag{13}$$

The initial conditions are assumed as

$$N(r, z, 0) = \begin{cases} N_H/N^*, & 0 < r < a/R, \\ 1, & a/R < r < 1, \end{cases} \tag{14}$$

$$M(r, z, 0) = 0, \tag{15}$$

$$\phi(r, z, 0) = \tanh\frac{r - a/R}{2\sqrt{2}\epsilon}. \tag{16}$$

Boundary condition	$r = 1$ and $z = H/R$
Case (1)	$N = 1$
Case (2)	$N = N_H/N^*$

We denote Case (1) given as the boundary condition for the nutrient $N = 1$ and Case (2) given as $N = N_H/N^*$ on $r = 1$ and $z = H/R$. Case (1) implies the lack of nutrient supply and Case (2) is abundant nutrient supply.

3 Numerical Solution

We employ a finite difference method to solve the nutrient concentration $N(r, z, t)$, the newly generated matrix $M(r, z, t)$, and the order parameter $\phi(r, z, t)$ in the cylindrical coordinates (r, z). Let us first discretize the given computational domain $\Omega = (0, 1) \times (0, H/R)$ as a uniform grid with a space step $h = 1/N_r = H/(RN_z)$ and a time step $\Delta t = T/N_t$ for a total time T. Let $[0, 1]$ and $[0, H/R]$ be partitioned by

$$0 = r_{1/2} < r_{1+1/2} < \cdots < r_{N_r+1/2} = 1,$$
$$0 = z_{1/2} < z_{1+1/2} < \cdots < z_{N_z+1/2} = H/R$$

then the cells I_{ik} cover $\Omega = [0, 1] \times [0, H/R]$. Let $\Omega_h = (r_i, z_k)$ be the set of cell-centers where

$$r_i = (r_{i-1/2} + r_{i+1/2})/2, \quad z_k = (z_{k-1/2} + z_{k+1/2})/2.$$

We assume M, N and ϕ are on the cell-centers. The numerical approximations of the solution are denoted as

$$N_{ik}^n \equiv N(r_i, z_k, t_n) = N\big((i-0.5)h, (k-0.5)h, n\Delta t\big), \tag{17}$$

$$M_{ik}^n \equiv M(r_i, z_k, t_n) = M\big((i-0.5)h, (k-0.5)h, n\Delta t\big), \tag{18}$$

$$\phi_{ik}^n \equiv \phi(r_i, z_k, t_n) = M\big((i-0.5)h, (k-0.5)h, n\Delta t\big), \tag{19}$$

where $i = 1, \ldots, N_r$, $k = 1, \ldots, N_z$, and $n = 0, \ldots, N_t$. Here N_r, N_z, and N_t are the number of nodes for r, z, and t directions, respectively. We define the discrete differentiation operator as $\nabla_h \phi_{i+\frac{1}{2},k} = (\phi_{i+1,k} - \phi_{ik})/h$, $\nabla_h \phi_{i,k+\frac{1}{2}} = (\phi_{i,k+1} - \phi_{ik})/h$ and the discrete Laplacian operator as $\Delta_h \phi_{ik} = (\nabla_h \phi_{i+\frac{1}{2},k} - \nabla_h \phi_{i-\frac{1}{2},k} + \nabla_h \phi_{i,k+\frac{1}{2}} - \nabla_h \phi_{i,k-\frac{1}{2}})/h$. Using the above notations, we solve Eqs. (11) and (12) using a hybrid numerical scheme based on the operator splitting scheme (Li et al. 2010). This operator splitting method divides its differential operator into the first order ordinary differential equations which are solved analytically and implicitly. With following two steps, we have N_{ik}^{n+1} and M_{ik}^{n+1} from initially given N_{ik}^n and M_{ik}^n.

Step (1) The following first order ordinary differential equations are solved analytically using N_{ik}^n and M_{ik}^n:

$$N_t = -\Gamma_N(\phi)(N-1)(\delta - M), \qquad M_t = \Gamma_M(\phi)(N-1)(\delta - M). \tag{20}$$

Then we have

$$N_{ik}^{n+\frac{1}{2}} = 1 + \big(N_{ik}^n - 1\big)e^{\Gamma_N(\phi_{ik}^n)(M_{ik}^n - \delta)\Delta t}, \tag{21}$$

$$M_{ik}^{n+\frac{1}{2}} = \delta + \big(M_{ik}^n - \delta\big)e^{\Gamma_M(\phi_{ik}^n)(1 - N_{ik}^n)\Delta t}. \tag{22}$$

Step (2) The diffusion equations are discretized using the implicit scheme as follows:

$$\begin{aligned}
\frac{N_{ik}^{n+1} - N_{ik}^{n+\frac{1}{2}}}{\Delta t} = {} & \frac{D_N(\phi^n_{i+\frac{1}{2},k}) r_{i+\frac{1}{2},k}}{h^2 r_{ik}} \big(N_{i+1,k}^{n+1} - N_{ik}^{n+1}\big) \\
& - \frac{D_N(\phi^n_{i-\frac{1}{2},k}) r_{i-\frac{1}{2},k}}{h^2 r_{ik}} \big(N_{ik}^{n+1} - N_{i-1,k}^{n+1}\big) \\
& + \frac{D_N(\phi^n_{i,k+\frac{1}{2}})}{h^2} \big(N_{i,k+1}^{n+1} - N_{ik}^{n+1}\big) \\
& - \frac{D_N(\phi^n_{i,k-\frac{1}{2}})}{h^2} \big(N_{ik}^{n+1} - N_{i,k-1}^{n+1}\big),
\end{aligned} \tag{23}$$

$$\begin{aligned}\frac{M_{ik}^{n+1}-M_{ik}^{n+\frac{1}{2}}}{\Delta t} &= \frac{D_M(\phi^n_{i+\frac{1}{2},k})r_{i+\frac{1}{2},k}}{h^2 r_{ik}}\big(M^{n+1}_{i+1,k}-M^{n+1}_{ik}\big)\\ &\quad - \frac{D_M(\phi^n_{i-\frac{1}{2},k})r_{i-\frac{1}{2},k}}{h^2 r_{ik}}\big(M^{n+1}_{ik}-M^{n+1}_{i-1,k}\big)\\ &\quad + \frac{D_M(\phi^n_{i,k+\frac{1}{2}})}{h^2}\big(M^{n+1}_{i,k+1}-M^{n+1}_{ik}\big)\\ &\quad - \frac{D_M(\phi^n_{i,k-\frac{1}{2}})}{h^2}\big(M^{n+1}_{ik}-M^{n+1}_{i,k-1}\big).\end{aligned} \tag{24}$$

We use a multigrid method to solve Step (2) (Briggs 1987; Trottenberg et al. 2001) and a numerical method introduced in Shin et al. (2011) is applied to have the values of D_N and D_M.

To solve the governing equation (13) efficiently, we propose a hybrid numerical scheme using the operator splitting scheme (Li et al. 2010). We introduce the intermediate variable ϕ^* and ϕ^{**} to split the operator. Our hybrid method for ϕ proceeds with following three steps:

Step (1) For the first order ordinary differential equation, we solve the following equation using ϕ^n_{ik}:

$$\phi_t = \frac{\sqrt{2}\beta}{2\epsilon}\big(\delta + M^n_{ik}\big)\sqrt{F\big(\phi^n_{ik}\big)}. \tag{25}$$

Then we have the analytic solution by using the separation of variables as follows:

$$\phi^*_{ik} = \frac{\phi^n_{ik}-1+(\phi^n_{ik}+1)e^{\sqrt{2}\beta(\delta+M^n_{ik})\Delta t/\epsilon}}{-\phi^n_{ik}+1+(\phi^n_{ik}+1)e^{\sqrt{2}\beta(\delta+M^n_{ik})\Delta t/\epsilon}}.$$

Step (2) $\phi_t = \alpha(\delta+M)\Delta\phi$ is solved implicitly using ϕ^*_{ik} as follows:

$$\frac{\phi^{**}_{ik}-\phi^*_{ik}}{\Delta t} = \alpha\big(\delta + M^n_{ik}\big)\Delta_h\phi^{**}_{ik}. \tag{26}$$

To solve Step (2), we use the multigrid method (Briggs 1987; Trottenberg et al. 2001).

Step (3) For the first order ordinary differential equation, we solve the following equation using ϕ^*_{ik}:

$$\phi_t = -\frac{\alpha}{\epsilon^2}(\delta+M)F'(\phi). \tag{27}$$

Then we have the analytic solution by using the separation of variables as follows:

$$\phi^{n+1}_{ik} = \frac{\phi^{**}_{ik}}{\sqrt{e^{-2\alpha(\delta+M^n_{ik})\Delta t/\epsilon^2}+(\phi^{**}_{ik})^2(1-e^{-2\alpha(\delta+M^n_{ik})\Delta t/\epsilon^2})}}.$$

The solution of Step (1)–Step (3) allows to obtain ϕ^{n+1}_{ik} from the given ϕ^n_{ik}.

Table 1 Parameter set for level set (Olson and Haider 2009) and phase-field

Cases	Mean curvature	Speed of moving interface
Level set	0.0001 or 0.0005	0.001 or 0.005
Phase-field	$\alpha = 0.0001$ or 0.0005	$\beta = 0.001$ or 0.005

4 Numerical Results

In this section, we present numerical results for spatial and temporal articular cartilage regenerations using our proposed model. Our numerical results include the parameter set for the phase-field model comparing with the level set, convergence test, temporal evolution of the N, M, and ϕ with different nutrient supply, different matrix synthesis rate, and magnitude of defected region. For the diffusion coefficient, we impose ten times higher values for hydrogel than cartilage (Nettles et al. 2004) as the nutrient concentration is water-rich whereas most of cartilage is comprised largely of collagen fibers (Leddy and Guilak 2003). A reference value is $D_N^- = 8000\ \mu m^2/s$ which lies in the range of 600–8000 $\mu m^2/s$ (Nettles et al. 2004). In articular cartilage, the range of diffusion coefficients was 50–70 $\mu m^2/s$ (Nettles et al. 2004). Therefore, diffusion coefficients $D_N^- = 1$, $D_N^+ = 0.01$, $D_M^- = 0.1$, and $D_M^+ = 0.001$ (Olson and Haider 2009) are used, unless otherwise specified where a reference value is $D_N^- = 1$ from the nondimensionalization. $H/R = 1$, $a/R = 0.5$, and a constant $\epsilon = 8h/(2\sqrt{2}\tanh^{-1}(0.9))$ are considered. We assume that $M_{\max} = 2M^*$ then we have $\delta = 2$. The nutrient rich hydrogel N_H has ten times higher nutrient concentration of cartilage at homeostasis N^*, that is $N_H/N^* = 10$. As the values of γ_N and γ_M are not available experimentally, we vary γ_M to demonstrate the effect of γ_M and $\gamma_N = 0.01$ is used. Numerical solutions are calculated on the computational domain $\Omega = (0, 1) \times (0, 1)$. For whole numerical simulations, the interface ϕ is captured at the level 0.

4.1 Parameter Set for Phase-Field Model

We numerically determine the values of parameter α and β for Eq. (13). Here, we fix $M = 0$ to compare the theoretical values. When $\alpha = 1$ and $\beta = 0$ (see Fig. 5(a)), ϕ follows the mean curvature and R satisfies theoretical value $R(t) = \sqrt{0.25 - 2t}$ (Li et al. 2010) on the radially symmetric domain. When $\alpha = 0$ and $\beta = 1$ (see Fig. 5(b)), the speed of the moving interface is 1 as the traveling wave solution of ϕ is $\phi = \tanh(x - t)/\sqrt{2}\epsilon$. Remark that the temporal aggregation speeds up to the core by the effect of axisymmetric domain and this behavior will be shown in the rest of the simulations.

To match the parameter set for the phase-field method, we compare the parameter set from the level set method (Olson and Haider 2009) as Table 1.

Unless otherwise specified, we use scaled values $\alpha = 0.0001$ and $\beta = 0.001$.

4.2 Convergence Test

To verify the accuracy of our proposed scheme, we perform a convergence test with mesh refinements. Here, a fixed value $\epsilon = 0.015$ and nutrient source $N = 5$ are used.

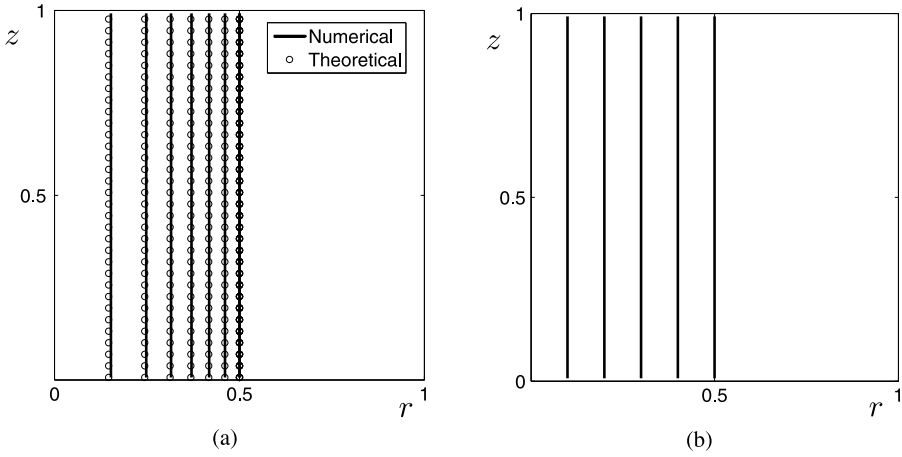

Fig. 5 Parameter set (**a**) mean curvature R where the *solid lines* represent the numerical results and *circles* show the theoretical results for α and (**b**) speed of the moving interface at $T = 0.1$ for β

Fig. 6 Convergence test with mesh refinements

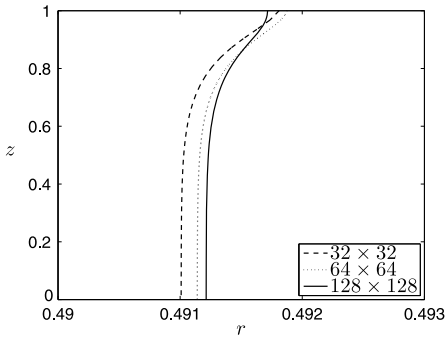

We use finer spatial mesh sizes up to four levels, such as, $h = 1/2^n$ for $n = 6, 7, 8$, and 9. For each mesh size, numerical calculation is run until the time $T = 0.1$ with the time step size $\Delta t = 0.001h$. The overlapped contour of ϕ is calculated with 64×64, 128×128, 256×256 and 512×512 spatial grid nodes. The convergence of our proposed scheme is clearly observed with mesh refinements in Fig. 6.

4.3 Sensitivity Study

Numerical simulations with varying values of γ_M and supply of the nutrient source are performed to investigate the regeneration time and hydrogel environment. The fixed values $\gamma_N = 0.01$, $\alpha = 0.01$, and $\beta = 0.1$ are used and numerical solutions are computed with a spatial step size $h = 1/64$ and a temporal step size $\Delta t = 0.005$. In this section, the overlapped temporal evolution of ϕ at the level 0 is drawn with 11 intervals from initial to final time.

The result presented in Fig. 7 shows how the matrix synthesis rate γ_M and the nutrient source influence to the regeneration time and spatial cartilage-hydrogel aggregation. As the growth factors affect on the rate of matrix synthesis, different values of

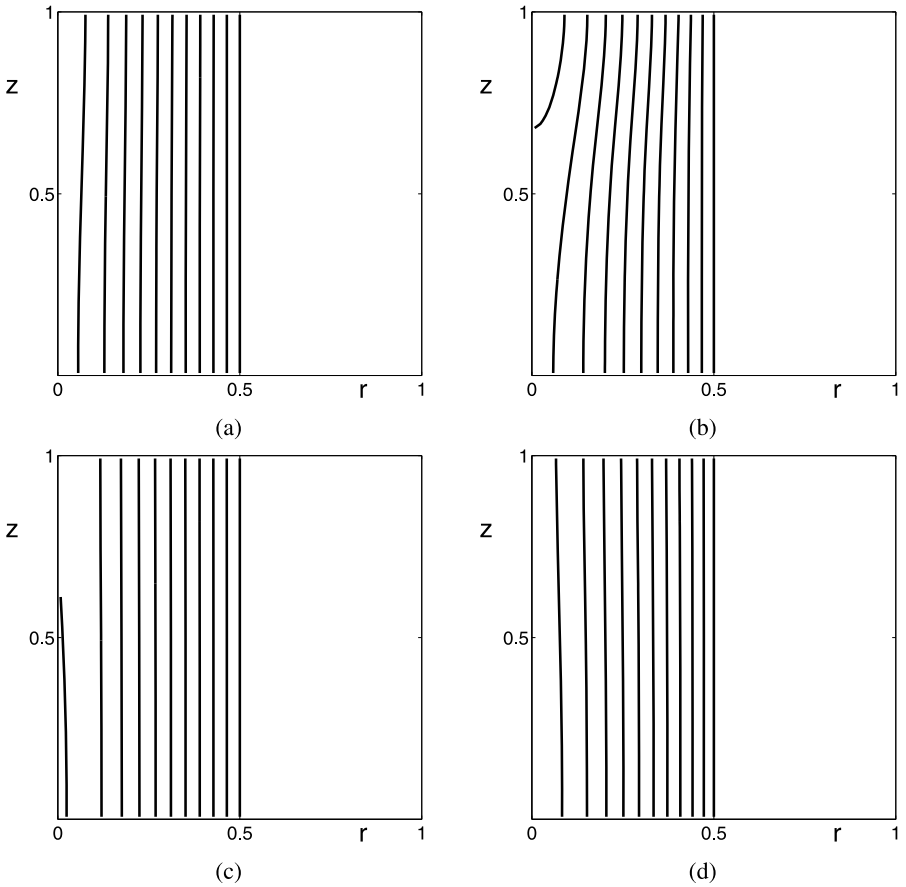

Fig. 7 Overlapped temporal evolution of ϕ for Case (1), (**a**) $\gamma_M = 0.05$, $T = 1.5$, and (**b**) $\gamma_M = 1$, $T = 1.25$. For Case (2), (**c**) $\gamma_M = 0.05$, $T = 1.5$, and (**d**) $\gamma_M = 1$, $T = 1.05$

γ_M are simulated. When the nutrient supply is restricted, Case (1), a small value of the matrix synthesis rate $\gamma_M = 0.05$ needs to evolve until the total time $T = 1.5$ whereas twenty times higher matrix synthesis rate $\gamma_M = 1$ totally aggregates in $T = 1.25$. The interface is advected largely along the top region, which shows slow regeneration at the top which occurs by a limited nutrient source. We observe that regeneration processes are almost similar whereas the total time for $\gamma_M = 1$ is almost 1.2 times faster than $\gamma_M = 0.05$. Therefore, the more the synthesis rate affects to the faster reaction speeds.

Next, we impose the sufficient nutrient supply Case (2) which is shown in the second row of Fig. 7. The results show consistent results from the previous test as the restricted synthesis rate (c) $\gamma_M = 0.05$ needs more total regeneration time $T = 1.5$ than (d) $\gamma_M = 1$ having the elapsed time $T = 1.05$. As supply of the nutrient is enough, the interface proceeds rapidly inward direction at the top. Temporally, (d) $\gamma_M = 1$ shows 1.4 times faster regeneration than (c) $\gamma_M = 0.05$ whereas the spatial regeneration shape is almost similar. By the nutrient sources, Case (2) is 1.19 times faster

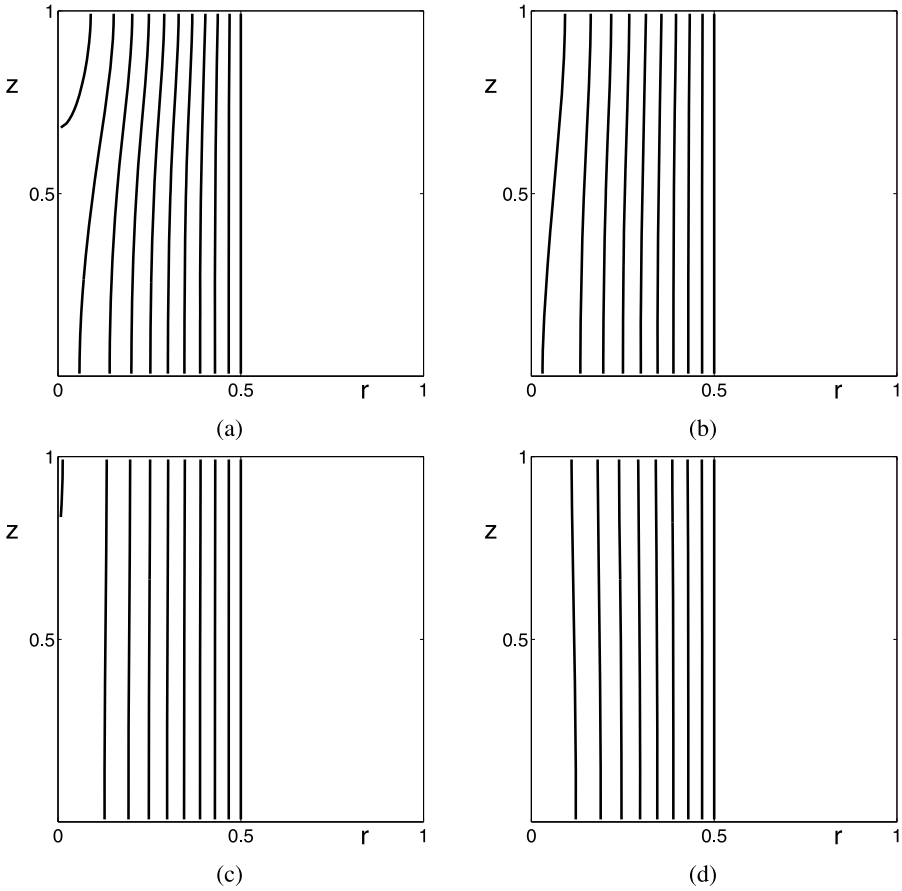

Fig. 8 Evolution of ϕ with boundary conditions (**a**) Case (1), (**b**) $N = 4$, (**c**) $N = 7$, and (**d**) Case (2)

than Case (1). Overall, we observe that a supply of nutrient affects to the spatial regeneration and increasing values of reaction terms speeds up the evolution.

We consider the spatial control with varying nutrient supply by different material properties of hydrogels. The boundary conditions (a) Case (1), (b) $N = 4$, (c) $N = 7$, and (d) Case (2) are considered for the total time $T = 1.25$.

The other parameters are the same as the previous section. The result in Fig. 8 reveals that increasing nutrient supply is obviously affects to the faster spatial and temporal regenerations. Due to the nutrient source, cartilage tissue aggregates to the core with higher speed at the top with sufficient nutrients. Depending on the geometry of cartilage damage, controlled spatial regeneration is able to be considered.

4.4 Temporal Evolution of N, M and ϕ

We illustrate the temporal evolution of N, M and ϕ with Case (1) and Case (2) to observe the nutrient consumption and matrix aggregation. Parameters $\gamma_M = 1$,

$\gamma_N = 0.01$, $\alpha = 0.01$, and $\beta = 0.1$ are chosen. Numerical solutions are computed with uniform space mesh $h = 1/64$ and the time step $\Delta t = 0.0005$.

First, temporal evolutions of N, M and ϕ with the boundary condition Case (2) are simulated. Figure 9(a) shows the overlapped temporal evolution of ϕ with 11 intervals from initial to final time (the total time $T = 1.075$ is used). Results (b) show the nutrient concentration N at $t = 0$ (second row), $T/2$ (third row), T (fourth row), and (c) illustrate M at $t = T/10$ (top row), $T/2$ (second row) and T (bottom row), respectively. The bottom line on the rz-plane in (b) shows the contour of the interface ϕ at each corresponding time. Results (d) show interface ϕ at $t = 0$ (second row), $T/2$ (second row), T (fourth row), respectively. The aggregation of interface ϕ goes to the inward direction incorporating with the evolution of M. As the nutrient supplies enough, the repair process at the top region speeds up than the bottom region. By the effect of Dirichlet boundary on the boundary, N has substantially higher at the boundary and becomes evenly distributed. M has the relatively high concentration at the interfacial region as shown with the overlapped thicker dark line. Then the bottom row of Fig. 9 represents $\phi = 0$ isosurface of 3D configurations, which is obtained by replacing the axisymmetric domain to three-dimensional geometry and corresponding to ϕ at $t = T/10$, $T/3$, $T/2$, and T from the left to the right, respectively. The lasting repair of cartilage is visually demonstrated.

Next, the boundary condition Case (1) is investigated with the total time $T = 1.25$. The other parameters are the same as the previous test and the results shown in Fig. 10 are arranged with the same order of Fig. 9. These results suggest that the speed of turnover, captured with ϕ, is faster at the bottom region relative to the top region by the lack of nutrient supply. Moreover, M has high concentration at the interfacial region, which is the same as the previous test. However, the region near the boundary of M shows relatively low density by the lack of the nutrient supply. Though the temporal cartilage repair process slowly occurs compared to Fig. 9, the complete regeneration is observed.

4.5 Effect of Damaged Magnitude

Effects of the defective sizes are investigated by varying the initial conditions of the interface ϕ. The boundary condition Case (2) is adopted. Numerical solutions are computed with a uniform space mesh $h = 1/64$ and the time step $\Delta t = 0.0009$.

The different defective sizes are assumed such as $a/R = 0.25$ and $a/R = 0.75$. The overlapped temporal evolutions of ϕ from initial to final time with 9 intervals are shown in Fig. 11 (a) $a/R = 0.25$ with the total time $T = 1.35$ and (b) $a/R = 0.75$ with the total time $T = 2.25$. The consistent spatial evolutions are observed regardless of the defective sizes and the temporal evolution shows almost similar pattern in spite that small defective cartilage regenerates faster.

Next, restricted nutrient consumption of hydrogel is investigated in the simulation. The initial conditions for ϕ is given as

$$\phi(r, z, 0) = \begin{cases} -1, & r - z < 0.7, \\ 1, & \text{otherwise.} \end{cases}$$

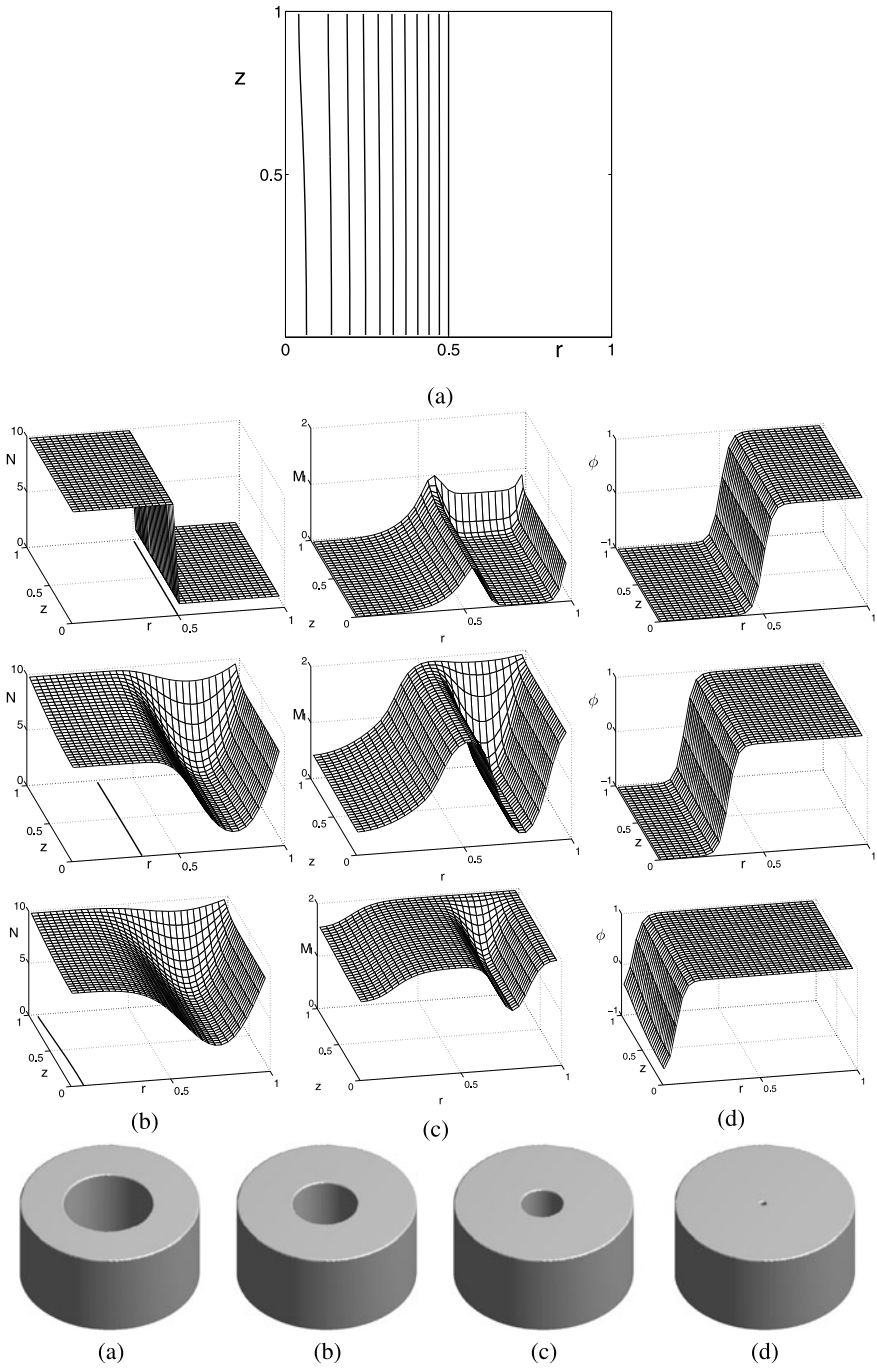

Fig. 9 Spatial and temporal aggregation of Case (2) : (**a**) overlapped 11 temporal evolution of ϕ (level 0). (**b**) N, (**c**) M, and (**d**) ϕ at time $t = 0$ (*second row*), $t = T/2$ (*third row*), and $t = T$ (*fourth row*). *Bottom row*: Corresponding 3D configuration (*bottom row*) for (**a**) $T/10$, (**b**) $T/3$, (**c**) $T/2$, and (**d**) T ($T = 1.075$)

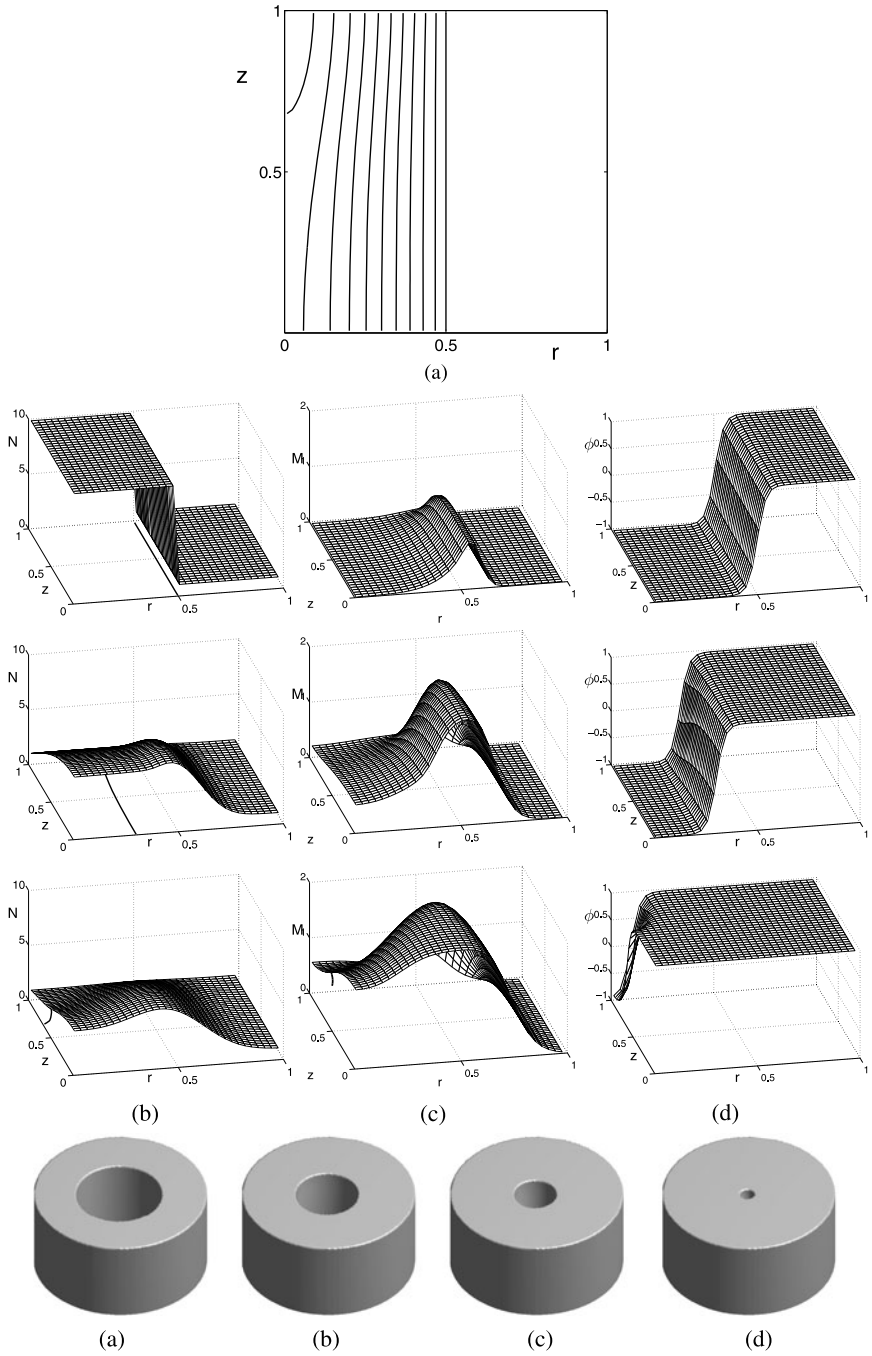

Fig. 10 For $\gamma_M = 1$ and $\gamma_N = 0.01$ with Case (1): (**a**) overlapped 11 temporal evolution of ϕ. (**b**) N, (**c**) M, and (**d**) ϕ at time $t = 0$ (*second row*), $t = T/2$ (*third row*), and $t = T$ (*fourth row*). *Bottom row*: Corresponding 3D configuration (*bottom row*) for $T/10$, $T/3$, $T/2$, and T ($T = 1.25$)

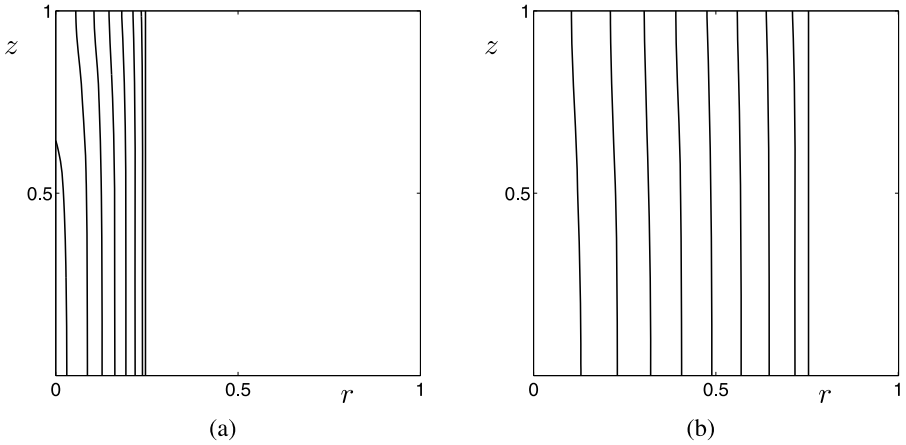

Fig. 11 Interface ϕ with different defective sizes for (**a**) $a/R = 0.25$ and (**b**) $a/R = 0.75$

With a temporal step size $\Delta t = 0.001$, we simulated temporal evolutions of N, M, and ϕ, and the same arrangement as simulations in Sect. 4.4 are used for results in Fig. 12. Likewise.. the previous investigation, M has high concentration at the interfacial region. The complete regeneration is able to be occurred regularly though relatively small proportion of nutrient source is supplied from the boundary.

Note that we fix the volume fraction of hydrogel as $\pi/8$ in Case (2) and the temporal evolutions of hydrogel-volume fractions are investigated. We consider the cylindrical shape, the truncated cones with gradients $m = -1$ (lack of nutrient supply) and $m = 1$ (adequate nutrient supply). Overall, we fix the nutrient concentration as 5. Then resulted volume fraction of scaffold on Fig. 13 explains that a cone shape with the gradient of 1 shows the rapid regeneration whereas the lack of nutrient supply results in the slow regeneration process.

5 Conclusions

We have proposed the phase-field method as a mathematical modeling for articular cartilage regeneration in degradable scaffolds. The spatial and temporal control of cartilage repair process is simulated using the mathematical modeling. The phase-field model simulates the hydrogel and cartilage interface where hydrogel turns into newly generated cartilage which has been studied by using the level set method (Olson and Haider 2009). Both the phase-field and level set methods simulate the dynamics involving a transitional region and approach to the equilibrium. However, the level set method could distort the dynamics, while the phase-field method keeps the same dynamics in numerics as those in the continuum PDEs in image problems. The phase-field model improves the numerical stability, where we proposed an unconditionally stable hybrid method, and eliminates the renormalization procedure.

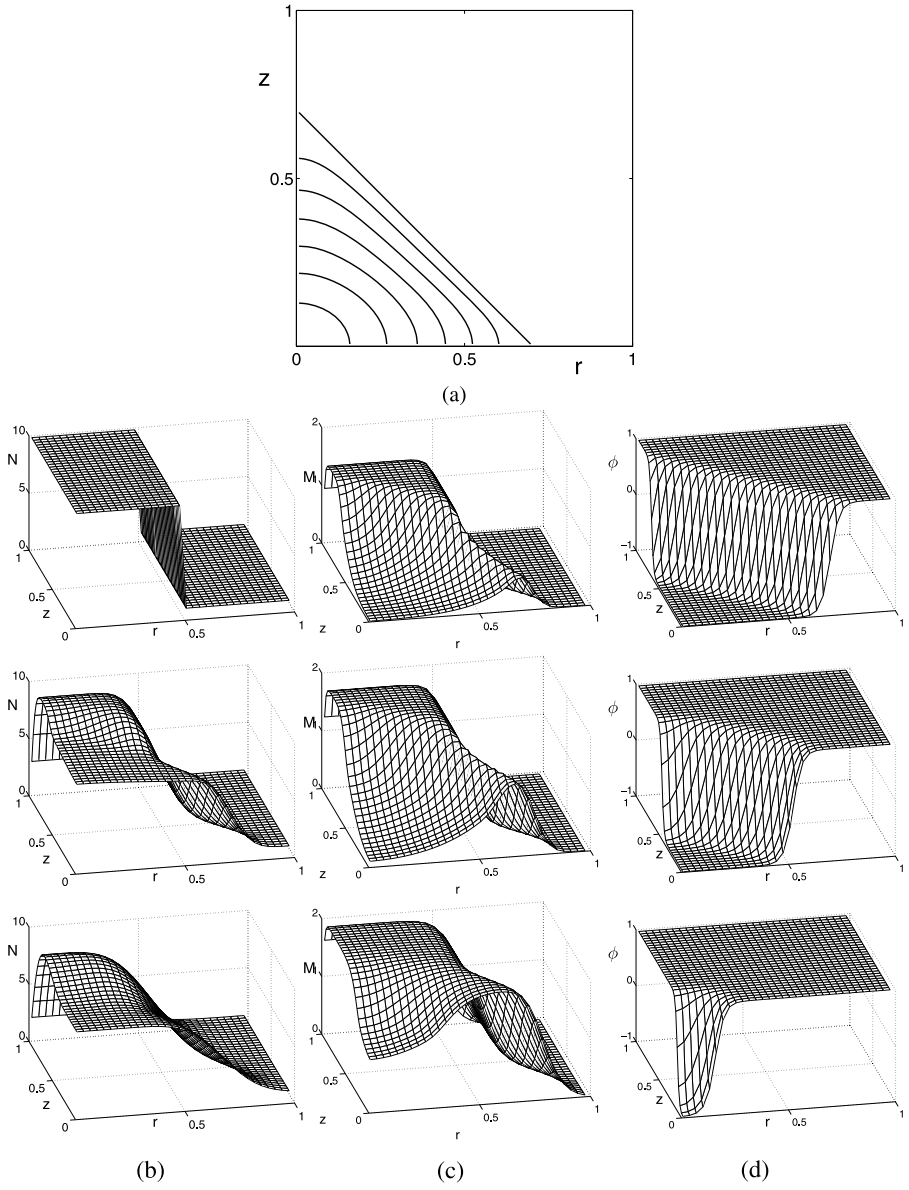

Fig. 12 (**a**) Overlapped 11 temporal evolution of ϕ. (**b**) N, (**c**) M, and (**d**) ϕ at time $t = 0$ (*second row*), $t = T/2$ (*third row*), and $t = T$ (*bottom row*) ($T = 0.75$)

In the modeling, a reaction-diffusion system is embedded to describe the nutrient and newly generated matrix. To explain the regeneration process, we have presented an unconditionally stable hybrid numerical method. We investigated convergence of our proposed numerical method, the effect of parameters which can be varied by hy-

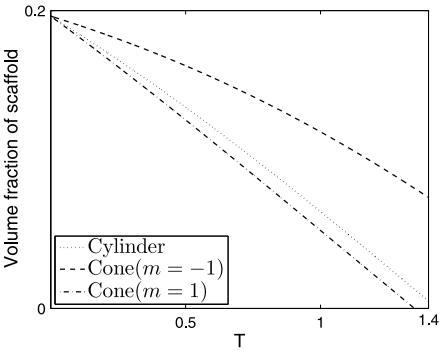

Fig. 13 Volume fraction of scaffold with cylindrical shape (*dotted line*), truncated cone with -1 (*dashed line*), and truncated cone with 1 (*dashed-dot line*)

drogel mechanical properties and cartilage environment. Moreover, we consider the regeneration time of cartilage and the potential improvement of hydrogel structures.

The simulated results were obtained with parameter values having experimental properties of hydrogel for providing nutrients supply which is interested biological field (Shakeel et al. 2013). The nutrient supply and physical magnitude of detected region affect to the time and spatial regeneration process. We expect our model gives guide as an in vitro experiment with the different initial shapes and material properties. As the diffusive interface models are in consistent with the statistical, physics, and thermodynamics through the variational problems, the biological problems related to the physics are easier to corporate with the phase-field model. Therefore, we expect the seeded hydrogel, the important part of tissue engineering resulted in the overall performance of scaffolds (Li et al. 2001), could study with our approach.

Acknowledgements The first author (A. Yun) was supported by National Junior research fellowship from the National Research Foundation of Korea grant funded by the Korea government (No. 2011-00012258). The corresponding author (J.S. Kim) was supported by the National Research Foundation of Korea (NRF) grant funded by the Korea government (MEST) (No. 2011-0027580). The authors also wish to thank the anonymous referee for the constructive and helpful comments on the revision of this article.

References

Betre, H., Setton, L., Meyer, D., & Chilkoti, A. (2002). Characterization of a genetically engineered elastin-like polypeptide for cartilaginous tissue repair. *Biomacromolecules*, *3*, 910–916.

Briggs, W. L. (1987). *A multigrid tutorial*. Philadelphia: SIAM.

Burkitt, H. G., Young, B., & Heath, J. W. (1993). *Functional histology* (3rd ed.). Edinburgh: Churchill.

Darling, E. M., & Athanasiou, K. A. (2003). Articular cartilage bioreactor and bioprocesses. *Tissue Eng.*, *9*, 9–26.

Davis, K. A., Burdick, J. S., & Anseth, K. S. (2003). Photoinitiated crosslinked degradable copolymer networks for tissue engineering applications. *Biomaterials*, *24*, 2485–2495.

Elisseeff, J., Anseth, K., Sims, D., McIntosh, W., Randolph, M., Yaremchuk, M., & Langer, R. (1999). Transdermal photopolymerization of poly(ethylene oxide)-based injectable hydrogels for tissue-engineered cartilage. *Plast. Reconstr. Surg.*, *104*, 1014–1022.

Freed, L. E., Marquis, J. C., Langer, R., & Vunjak-Novakovic, G. (1994). Kinetics of chondrocyte growth in cell-polymer implants. *Biotechnol. Bioeng.*, *43*, 597–604.

Galban, C. J., & Locke, B. R. (1997). Analysis of cell growth in a polymer scaffold using a moving boundary approach. *Biotechnol. Bioeng.*, *56*, 422–432.

Gao, L.-T., Feng, X.-Q., & Gao, H. (2009). A phase field method for simulating morphological evolution of vesicles in electric fields. *J. Comput. Phys.*, *228*, 4162–4181.

Glimm, T., Zhang, J., Shen, Y.-Q., & Newman, S. A. (2012). Reaction-diffusion systems and external morphogen gradients: the two-dimensional case, with an application to skeletal pattern formation. *Bull. Math. Biol.*, *74*, 666–687.

Grote, M. J., Palumberi, V., Wagner, B., Barbero, A., & Martin, I. (2011). Dynamic formation of oriented patches in chondrocyte cell cultures. *J. Math. Biol.*, *63*, 757–777.

Jackson, D. W., Lalor, P. A., Aberman, H. M., & Simon, T. M. (2001). Spontaneous repair of full-thickness defects of articular cartilage in a goat model. a preliminary study. *J. Bone Jt. Surg. Am.*, *83*, 53–64.

Kooi, B. W., Auger, P., & Poggiale, J. C. (1998). Aggregation methods in food chains. *Math. Comput. Model.*, *27*, 109–120.

Kuo, Y., & Tsai, Y.-T. (2010). Inverted colloidal crystal scaffolds for uniform cartilage regeneration. *Biomacromolecules*, *11*, 731–739.

Leddy, H. A., & Guilak, F. (2003). Site-specific molecular diffusion in articular cartilage measured using fluorescence recovery after photobleaching. *Ann. Biomed. Eng.*, *31*, 753–760.

Li, Y., Ma, T., Kniss, D. A., Lasky, L. C., & Yang, S. T. (2001). Effects of filtration seeding on cell density, spatial distribution, and proliferation in nonwoven fibrous matrices. *Biotechnol. Prog.*, *17*(5), 935–944.

Li, Y., Lee, H. G., Jeong, D., & Kim, J. S. (2010). An unconditionally stable hybrid numerical method for solving the Allen–Cahn equation. *Comput. Math. Appl.*, *60*, 1591–1606.

Murray, J. D. (2002). *Mathematical biology*. Berlin: Springer.

Min, C. (2010). On reinitializing level set functions. *J. Comput. Phys.*, *229*, 2764–2772.

Nettles, D. L., Parker Vail, T., Morgan, M., Grinstaff, M., & Setton, L. (2004). Photocrosslinkable hyaluronan as a scaffold for articular cartilage repair. *Ann. Biomed. Eng.*, *32*, 391–397.

Nguyen, K. T., & West, J. L. (2002). Photopolymerizable hydrogels for tissue engineering applications. *Biomaterials*, *23*, 4307–4314.

Noguchi, T., Yamamuro, T., Oka, M., Kumar, P., Kotoura, Y., Hyonyt, S. H., & Ikadat, Y. (1991). Poly (vinyl alcohol) hydrogel as an artificial articular cartilage: evaluation of biocompatibility. *J. Appl. Biomater.*, *2*, 101–107.

Olson, S. D., & Haider, M. A. (2009). A level set reaction-diffusion model for tissue regeneration in a cartilage-hydrogel aggregate. *Int. J. Pure Appl. Math.*, *53*, 333–353.

Ossendorf, C., Kaps, C., Kreuz, P., Burmester, G., Sittinger, M., & Erggelet, C. (2007). Treatment of posttraumatic and focal osteoarthritic cartilage defects of the knee with autologous polymer-based three-dimensional chondrocyte grafts: 2-year clinical results. *Arthritis Res. Ther.*, *9*, R41.

Rydholm, A. E., Bowman, C. N., & Anseth, K. S. (2005). Degradable thiol-acrylate photopolymers: polymerization and degradation behavior of an in situ forming biomaterial. *Biomaterials*, *26*, 4495–4906.

Sanz-Herrera, J. A., Garcia-Aznar, J. M., & Doblare, M. (2009). On scaffold designing for bone regeneration: a computational multiscale approach. *Acta Biomater.*, *5*, 19–29.

Sengers, B. G., Taylor, M., Please, C. P., & Oreffo, R. O. C. (2007). Computational modelling of cell spreading and tissue regeneration in porous scaffolds. *Biomaterials*, *28*(10), 1926–1940.

Shin, J., Jeong, D., & Kim, J. S. (2011). A conservative numerical method for the Cahn–Hilliard equation in complex domains. *J. Comput. Phys.*, *230*, 7441–7455.

Shakeel, M., Matthews, P. C., Graham, R. S., & Waters, S. L. (2013). A continuum model of cell proliferation and nutrient transport in a perfusion bioreactor. *Math. Med. Biol.*, *30*, 21–44.

Shirakawa, K., & Kimura, M. (2005). Stability analysis for Allen–Cahn type equation associated with the total variation energy. *Nonlinear Anal.*, *60*, 257–282.

Stile, R. A., Burghardt, W. R., & Healy, K. E. (1999). Synthesis and characterization of injectable poly(N-isopropylacrylamide)-based hydrogels that support tissue formation in vitro. *Macromolecules*, *32*, 7370–7379.

Taylor, J. E., & Cahn, J. W. (1998). Diffuse interfaces with sharp corners and facets: phase field models with strongly anisotropic surfaces. *Physica D*, *112*, 381–411.

Temenoff, J. S., & Mikos, A. G. (2000). Review: tissue engineering for regeneration of articular cartilage. *Biomaterials*, *21*, 431–440.

Trewenack, A. J., Please, C. P., & Landman, K. A. (2009). A continuum model for the development of tissue-engineered cartilage around a chondrocyte. *Math. Med. Biol.*, *26*(3), 241–262.

Trottenberg, U., Oosterlee, C., & Schüller, A. (2001). *Multigrid*. San Diego: Academic Press.

Wilson, C. G., Bonassar, L. J., & Kohles, S. S. (2002). Modeling the dynamic composition of engineered cartilage. *Arch. Biochem. Biophys.*, *408*, 246–254.

Wilson, D. J., King, J. R., & Byrne, H. M. (2007). Modelling scaffold occupation by a growing, nutrient-rich tissue. *Math. Models Methods Appl. Sci.*, *17S*, 1721–1750.

Yang, X., Feng, J. J., Liu, C., & Shen, J. (2006). Numerical simulations of jet pinching-off and drop formation using an energetic variational phase-field method. *J. Comput. Phys.*, *218*, 417–428.